SPE-212611-MS

Super-Resolution Reconstruction of Reservoir Saturation Map with Physical Constraints Using Generative Adversarial Network

Nandita Doloi, Somnath Ghosh, and Jyoti Phirani, Indian Institute of Technology Delhi, India

 DOI 10.2118/212611-MS

This paper was prepared for presentation at the SPE Reservoir Characterisation and Simulation Conference and Exhibition held in Abu Dhabi, UAE, 24 - 26 January 2023.

Abstract

Complete physics-based numerical simulations currently provide the most accurate approach for predicting fluid flow behavior in geological reservoirs. However, the amount of computational resources required to perform these simulations increase exponentially with the increase in resolution to the point that they are infeasible. Therefore, a common practice is to upscale the reservoir model to reduce the resolution such that numerous simulations, as required, can be performed within a reasonable time. The problem we are trying to solve here is that the simulation results from these upscaled models, although they provide a zoomed-out and global view of the reservoir dynamics, however, they lack a detailed zoomed-in view of a local region in the reservoir, which is required to take actionable decisions. This work proposes using super-resolution techniques, recently developed using machine learning methods, to obtain fine-scale flow behavior given flow behavior from a low-resolution simulation of an upscaled-reservoir model. We demonstrate our model on a two-phase, deal-oil, and heterogenous oil reservoir, and we reconstruct the oil saturation map of the reservoir. We also demonstrate how the network can be trained using dynamic coarse geological properties at various resolutions. The findings imply that even when coarse geological features and with limited resolution, the super-resolution reconstructions are able to recreate missing information that is close to the ground facts.

Introduction and Background

In recent years, there has been a lot of interest in forecasting dynamics in geological reservoirs. If we want to produce oil from the reservoir, we first have to forecast the amount of oil present in the reservoir and then perform a simulation to predict the amount we can produce from that reservoir. In CO_2 sequestration, we have to determine the storage of CO_2 for a particular aquifer and also to find out how much CO_2 we will be able to sequester in the aquifer. In Groundwater aquifers, we use several in-situ methods of remediation, which require forecasting of water composition after treatment. For all the above cases, we use numerical simulations because it is difficult to scale up analytical models with the increase in reservoir complexity. In Figure 1, we show the porosity profile of typical geological reservoirs, which shows the complexity of the geological system. These physics-based reservoir simulations that we use to understand

the flow and transport in the reservoirs are numerically very expensive. Our solution is based on super-resolution reconstruction; therefore, there is a need to increase the scale of dynamic properties of a reservoir, especially the saturation and pressure from coarse-scale to fine-scale. These properties are generally scalar or array of scalar values corresponding to each 3D unit cell representing a 3D volume of the reservoir. Thus, the values from unit cells of one layer are popularly represented as 2D images. To represent the values from unit cells of all layers, stacks of 2D images corresponding to each layer are used. This shows us that the values can be represented in the form of a 2D image, and it may be possible to employ super-resolution techniques as shown by Chaudhuri et al.(Chaudhuri, 2001) in Image Processing to increase the resolution of these images. To reiterate, super-resolution techniques are methods that take as input a low-resolution image and output a higher-resolution image. In the literature, this process is also closely related to downscaling (Brouwer and Fokker, 2013; Torrealba et al., 2019). Deep-learning and computer-vision are popularly used to solve these types of problem (Da Wang et al., 2021; Dong et al., 2015; Wang et al., 2018a; Ledig et al., 2017; Das et al., 2021). Moreover, super-resolution techniques have been used in related physical phenomena like fluid dynamics to enhance turbulent flow map (Bode et al., 2019; Fukami et al., 2019; Pant and Farimani, 2020). It is important to note that since our image represents physical phenomena, it may not be sufficient to just increase the resolution of the image without considering physical constraints such as the conservation of mass. Thus, we look at super-resolution methods specifically developed for reservoirs or porous media. Janssens et al. (Janssens et al., 2020) presented a method for the super-resolution of Computed Tomography scans of rock properties such as Porosity and Permeability. As mentioned before, it is required that we verify that the super-resolution image representing the physical properties does satisfy physical constraints. Therefore, Janssens et al.(Janssens et al., 2020) verify that the super-resolution rock properties have the desired behavior on Unsaturated and Two-Phase Fluid Flow. They (Janssens et al., 2020) employs a Generative Adversarial Neural Network (GAN), Wang et al.(Wang et al., 2019) employs a Convolution Neural Network (CNN). Purely statistical methods such as neighbor embedding algorithm have also shown promising results for the super-resolution reconstruction of CT scan images of rock samples as shown in (Wang et al., 2018b). However, all these methods only deal with static reservoir properties such as Porosity and Permeability. To the best of our knowledge, there is no related work on the super-resolution reconstruction of dynamic reservoir properties such as Saturation and Pressure. The methods employed for the super-resolution of static properties cannot be directly employed for that of dynamic properties because the dynamic properties need to be temporally consistent. For example, if a coarse-scale unit cell indicates that the oil saturation is 0.8, the set of finer-scale cells which replace the coarse-scale cell should in the aggregate, also have an oil saturation of 0.8, and if oil transfers from one cell to another from time t to t + 1, the fine-scale values have to satisfy mass transfer equations. Thus, there is a need for a method to reconstruct super-resolution images for dynamic reservoir properties which satisfy physical constraints. We can derive inspiration from Xie et al. (Xie et al., 2018), which presents a method for temporally consistent super-resolution reconstruction of fluid flow. However, this method is not specifically developed for flow through porous media where there are stricter physical constraints to satisfy, as described above. Super-resolution has also been employed in modeling Turbulence in Computational Fluid Dynamics. Pant et al. (Pant and Farimani, 2020) use a U-Net CNN architecture (Ronneberger et al., 2015) to perform the up-scaling of turbulence data and, most importantly, employ a physics-based loss function which ensures that the super-resolution reconstruction satisfies the conservation of kinetic energy and mass.

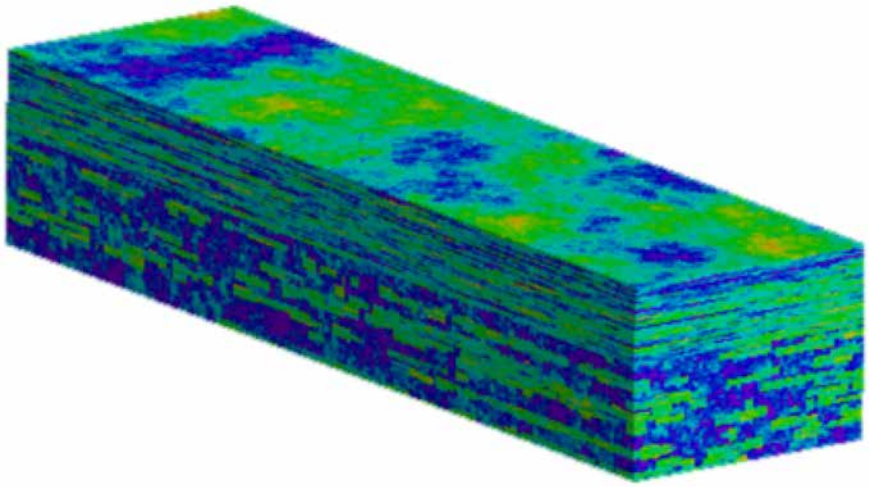

Figure 1—Visualization of a Reservoir Porosity.

Due to recent developments in big data and a slew of emergent Machine Learning applications in academia and industry, data-driven-based proxies have exploded in prominence in recent decades. This class of proxies takes a data-driven method in which a set of data observations is trained for reservoir forecasting without relying on any specific physical equation. The training data set for the model could be either from field observations or created with the help of a reservoir simulator. However, tree-based methods such as random forests and gradient boosting are widespread. Castelletti et al. 2010(Castelletti et al., 2010), most studies in this area have employed artificial neural networks (ANN) as the learning algorithm (Ahmadi et al. (2013)(Ahmadi et al., 2013)),(Yu, Zhu, and Diao 2008(Yu et al., 2008)). To estimate the connectivity, an artificial neural network (ANN) was used by Panda and Chopra (1998) (Panda et al., 1998). The network's inputs were injection rates (from a time window), permeability, and thickness, and the model's outputs were oil and water rates. By taking the partial derivative of oil production concerning the injection rate, they were able to quantify the relative influence of each injector on the producer. A sensitivity analysis based on a neural network was used by Demiryurek et al. (Demiryurek et al., 2008) to quantify the inter-well connectivity between injectors and producers in a reservoir. They evaluated the impact of the candidate injector on the target producer by varying the injection rates, i.e. the inputs to the trained neural network model, and analyzing the outputs (production rates). Hence, by a specific amount of injection rate change, if the production rate change is noticeable, that injector and producer are well connected. Shahkarami et al. citepshahkarami2020applications use smart proxy models in two cases; the first case investigated the application of a proxy model for calibrating a reservoir simulation model based on historical data and predicting well production, while the second study investigated the application of an ANN-based proxy model for fast-track modeling of CO2 enhanced oil recovery, aiming at the prediction of the reservoir pressure and phase saturation distribution at injection stage and post-injection stage. In line with the upcoming paradigm shift involving data-driven science, (Maula et al., 2020) this study aims to use data mining and artificial intelligence to investigate the conceptual framework, development, and feasibility of the data-driven approach in the Artificial Neural Network-based Grid-block Surrogate Reservoir Model (GSRM) Smart Proxy. The Smart Proxy model is applied for unconventional shale gas reservoirs with dynamic property response prediction output of grid-block pressure and gas saturation. A purely data-driven model is a black box and hence they are often not considered reliable enough to make expensive decisions. However, with the advent of concepts like theory-guided data science (Karpatne et al., 2017) and physics-informed neural networks (Cai et al., 2022), hybrid models, which are driven by both data and analytical models have become more popular as it allows these models to be more transparent and reliable.

Preliminaries

Upscaling a reservoir model Since oil is the most complex system where there can be multiple components, therefore, as an example, we describe the governing equations of flow in oil and gas reservoirs for forecasting production from these reservoirs. If we consider three phases in an oil reservoir i.e., oil, gas, and water, where oil and gas are miscible in each other and water is immiscible, then we have the following equations to solve.

$$\frac{\partial}{\partial t}\left[\phi\left(\frac{S_o}{B_o}+\frac{R_v S_g}{B_g}\right)\right]+\delta\cdot\left(\frac{1}{B_o}\vec{\mu}_o+\frac{R_v}{B_g}\vec{\mu}_g\right)=0. \tag{1}$$

$$\frac{\partial}{\partial t}\left[\phi\left(\frac{S_w}{B_w}\right)\right]+\delta\cdot\left(\frac{1}{B_w}\vec{\mu}_w\right)=0. \tag{2}$$

$$\frac{\partial}{\partial t}\left[\phi\left(\frac{R_s S_o}{B_o}+\frac{S_g}{B_g}\right)\right]+\delta\cdot\left(\frac{R_s}{B_o}\vec{\mu}_o+\frac{1}{B_g\vec{\mu}_g}\right)=0. \tag{3}$$

where ϕ is the porosity of the porous medium. S_w is a water saturation, S_o,S_g are saturation of liquid (oil) and vapor (gas) phases in the reservoir. $\vec{\mu}_o$, $\vec{\mu}_w$, $\vec{\mu}_g$ are Darcy velocities of the liquid phase, water phase, and vapor phase in the reservoir. B_o is an oil formation volume factor (ratio of some volume of reservoir liquid to the volume of oil at standard conditions obtained from the same volume of reservoir liquid). B_w is a water formation volume factor (ratio of the volume of water at reservoir conditions to the volume of water at standard conditions). B_g is a gas formation volume factor (ratio of some volume of reservoir vapor to the volume of gas at standard conditions obtained from the same volume of reservoir vapor). R_s is a solution of the gas in the oil phase (ratio of the volume of gas to the volume of oil at standard conditions obtained from some amount of liquid phase at reservoir conditions). R_v is a vaporized oil in the gas phase (ratio of the volume of oil to the volume of gas at standard conditions obtained from some amount of vapor phase at reservoir conditions).

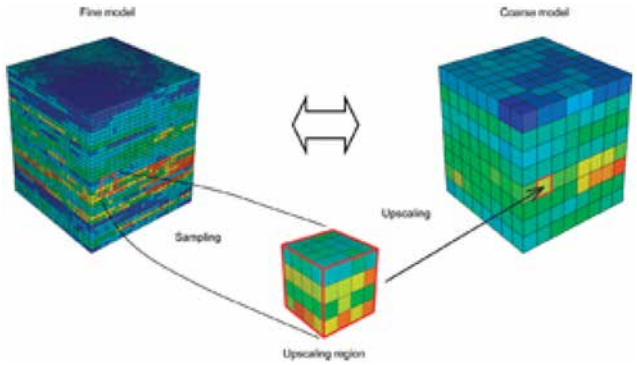

Figure 2—Conceptual illustration of the upscaling process.

This equation governing the flow of a fluid in a reservoir results from a combination of Darcy's law and the conservation of mass equation for that phase. Running the numerically expensive simulation to solve the above equations is also challenging. This is because (1) reservoirs are huge, and very large grids size is used for discretization, (2) the reservoirs are heterogeneous. Therefore multiple production scenarios are needed using different well locations or well-operating conditions, which makes the simulation task enormous (Liu and McVay, 2010). At present, (Britto et al., 2020) we can find several commercial software dedicated to oil reservoir simulations such as STARS of CMG, ECLIPSE-100 of Schlumberger, REVEAL of Petroleum Experts. ECLIPSE Compositional simulator (E300) is used for CO_2 sequestration. The main variables here are the pressure and the saturation of the wetting fluid, calculated by the implicit pressure

and explicit saturation (IMPES) method, where water pressure is the implicit variable, and water saturation is the explicit variable.

Petrophysical properties of geological reservoirs, such as porosity and permeability, are generally available on a fine scale. However, upscaling of these properties is required to attempt the numerical simulations due to the large size of these reservoirs. However, we see that upscaling leads to the loss of information and heterogeneity. Upscaling, or homogenization, is substituting a heterogeneous property region consisting of fine grid cells with an equivalent homogeneous region made up of a single coarse-grid cell with an effective property value. Equivalent, in this case, means either volume or flux must be the same in the fine-scale and upscaled model, depending on the type of property that is to be upscaled. Upscaling is performed for each of the cells in the coarse grid and each of the grid properties needed in the reservoir flow-simulation model. Therefore, the upscaling process is essentially an averaging procedure in which the static properties (Eg. Porosity and permeability) and dynamic properties(Eg: saturation and Pressure) characteristics of a fine-scale model are to be approximated by that of a coarse-scale model. A conceptual illustration of the upscaling process is shown in Figure 2.

Regardless of its flaws, the main advantage of upscaling a fine-scaled reservoir model is that the time required for the simulation reduces significantly, although the simulation results are now approximate. **Machine Learning** Machine learning techniques are a group of algorithms that can transform data into useful information. They are a type of approach in which solutions are derived primarily from data rather than physics-based models. Machine learning was first used in the mainstream in the 1990s, with the most popular example being the email spam filter (Lantz, 2019). Advances in computer processing capacity and machine intelligence have contributed to a wider wave of evolving big data applications in technology and business, including self-driving vehicles, facial recognition, text prediction, and natural language processing, over the last decade. While these machine learning models have shown tremendous success, it is important that we are aware of the inaccuracies of prediction and develop our algorithms around it, for example in (Das et al., 2022), the authors use high-fidelity simulation when the learned models may be inaccurate. Several authors have successfully used data-driven approaches to solve the challenges of geological reservoirs. Holdway et al. (Holdaway, 2014), and Cao et al. (Cao et al., 2016) use the popular machine learning algorithm Artificial Neural Network (ANN) to forecast production for existing and new wells in unconventional oil/gas reservoirs using inputs like geological maps, production history, pressure data, and operational constraints. The workflow entails using these data sets to train and refine the ANN model, which is then used to forecast the good output performance of both existing wells and new wells based on the history of neighboring wells drilled in similar geological locations. The results of the neural network model's final prediction were compared to those of the exponential, harmonic, and hyperbolic models, and the neural network achieved much more accurate predictions than the other three conventional empirical models.

The data-driven technique, which was used in reservoir studies, has various advantages and disadvantages. Linear Regression is very simple, computationally inexpensive, and used for quick, simple prediction of linear data. However, they are inaccurate in some cases and also use limited attributes in representation. Decision Trees are used for classification and regression analysis. It performs well, despite missing data and various kinds of data formats and is also pretty robust in the presence of noise. However, decision trees are prone to data overfitting data and also have a high number of attributes that can hurt the performance of the tree. Support Vector Machines(SVM) is used for non-linear and linear data sets with noisy data and give high-accuracy regression. SVM is even robust in the presence of data inaccuracies and fast evaluation of learned target function. It has a small drawback of computationally intensive training. Artificial neural network(ANN) is highly versatile and useful in parameter optimization, regression, and classification. ANN is robust in performance despite the noise, and the algorithm of ANN is highly durable and can maintain performance despite failure in a specific layer. However, for disadvantages, ANN is difficult in the interpretation of the procedure of obtaining results, and training the data is computationally

intensive. A simple structure of a neural network is shown in Figure 3 with a hidden layer and output. Genetic Algorithms(GA) are used for optimization, parameter selection, and when data is not uniform. It has high accuracy in parameter selection, low memory usage, and robustness despite outliers. GA is computationally intensive, and it has a probability of premature solution convergence.

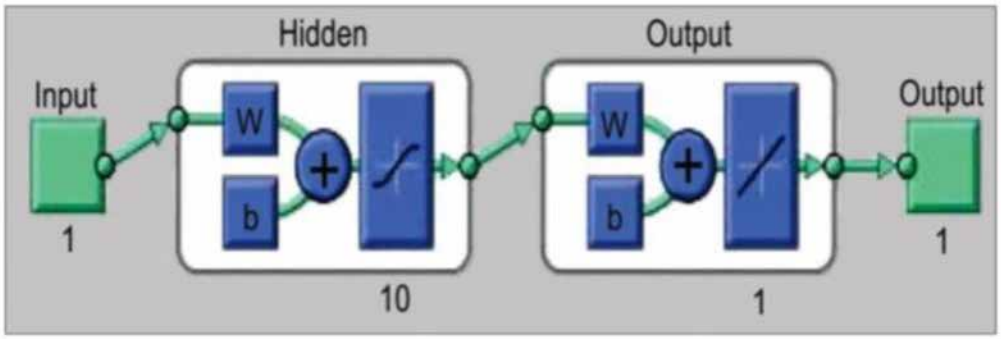

Figure 3—Simple neural network structure used in (Jia et al., 2016).

Machine learning, despite its enormous promise, has limitations. Most notably, it is largely incapable of extrapolating accurately outside of the ranges it has been trained (Lantz, 2019). The structuring and cleaning of large quantities of data is another major problem in machine learning applications (Rahm and Do, 2000). While this issue is not specific to machine learning algorithms, many datasets contain a high degree of obscure or redundant information that can negatively impact the performance of learning algorithms. ((Wuest et al., 2016)). Although machine learning approaches are often more realistic alternatives, they are not as accurate as complete physics solutions. Furthermore, most machine learning applications necessitate a large number of features to accurately replicate the output response surface. As a result, there are three major concerns: First, the dimensionality of the feature space increases the likelihood of extrapolation. Second, the amount of computing resources available grows exponentially.

Third, since these techniques rely on larger parameter spaces, they are more susceptible to overfitting. The realism of the forecasts is another major problem in machine learning applications.

Problem Formulation

The goal of this work is to develop a reconstruction method that satisfies hard physical constraints, such as conservation of mass, critical for dealing with saturation profiles.

Given a fine-scale two-phase, dead-oil reservoir model. Let the oil saturation map of the reservoir after simulation be S^{HR}. The saturation map is in the form of a rectangular grid where each layer along the z-axis is represented as a 2-D image I^{HR}. Thus, $S^{(\cdot)} = \{I_1^{(\cdot)}, I_2^{(\cdot)}, I_3^{(\cdot)}, \ldots, I_d^{(\cdot)}\}$ where d represents the number of layers in the saturation map. Now, let the saturation map of the same reservoir but using an upscaled model be S^{LR}. Hence, S^{LR} is a corresponding low-resolution version of S^{HR}. Similarly, for each layer i, I_i^{LR} is a low-resolution image corresponding to I_i^{HR}. However, unlike (Ledig et al., 2017), this low-resolution image is not generated from the high-resolution version. Instead, it is generated by another process. The correspondence is generated because both these images represent the same physical reservoir after simulation. Since the saturation map provides the ratio of the volume occupied by oil in each grid cell, we can compute the mass of the oil as shown in Equation 4. Thus, let the mass calculated from a given saturation map be $m(I^{LR})$.

Finally, the problem is to generate a high-resolution image I^{SR} given only the low-resolution image I^{LR} such that

1. The reconstruction closely approximates the true high-resolution image I^{HR}.

2. The reconstruction obeys conservation of mass, i.e. $m(I^{LR}) = m(I^{SR})$

Approach

In this work, we will build upon the super-resolution GAN (SRGAN) (Ledig et al., 2017), and find an efficient way to add the physical constraints.

Physical Constraints Constraints in Machine Learning optimization are usually in the form of soft constraints, i.e. as a component in the loss function which the algorithm attempts to minimize without the guarantee that the constraints will be satisfied. So, we add the mass-balance soft constraint such that the total oil mass of the reservoir according to the oil saturation reconstruction should be equal to the total mass of the reservoir according to the low-resolution saturation profile. To that end, we first compute the mass of oil m_o, given the oil saturation s_o in each grid-cell according to PVT relations Equation 4. In our case, we are dealing with two-phase flow and dead-oil.

$$\begin{aligned} \rho_o &= b_o(p_o) \times \rho S, o \\ m_o &= V_c \times \varphi \times \rho_o \times S_o \end{aligned} \tag{4}$$

where p_o = Pressure of oil, $\rho_{S,o}$ = Surface density of oil, ρ_o = Density of oil, $b_o(p_o)$ = Shrinkage factor of oil, s_o = Saturation of oil, ϕ = Rock porosity, V_c = Volume of a grid cell, v_o = Volume of oil and m_o = Mass of oil.

Why GANs?

Using the same terminology as used in the SR-GAN paper (Ledig et al., 2017), where I^{LR}, I^{HR} and I^{SR} are the low-resolution image, the corresponding high-resolution target image and the super-resolution reconstruction output of the Generator model respectively. The high-resolution images are only available during the training. In (Ledig et al., 2017) I^{LR} is obtained by applying a Gaussian filter to I^{HR} followed by downsampling. It is important to note here that this is not how we generate low-resolution images for the case of oil saturation. In our case, however, I^{HR} is obtained by running a fine-scale simulation with some initial reservoir conditions. The corresponding I^{LR} is obtained by running a coarse-scale simulation of the same reservoir but with upscaled values for the rock porosity and permeability. We use this method because this is how the data will be in a real-world application. This detail is important because the corresponding images I^{HR} and I^{LR} even though they belong to the same reservoir, initial conditions are obtained by running two independent simulations. As a result, these independent simulations do not ensure that the mass of oil remaining in the reservoir will be equal. This is an artifact of the dataset generation process, which definitely can be improved to ensure the ideal condition where the mass of oil should be equal in both I^{HR} and I^{LR}. We will definitely search for a better dataset-generation process. In our dataset, this discrepancy is not large, and the mass difference is around 3% of the mass in I^{LR}. Thus, we believe we can disregard this discrepancy and focus on the deliverable where we want our model to generate consistent reconstructions, i.e. the mass of oil in I^{SR} should be equal to that of I^{LR}. This deliverable is important because when someone uses our model for a oil saturation profile I^{LR}, the reconstruction I^{SR} should not show more or less amount of oil in the reservoir as compared to the input. The above information is critical to understand our GAN training strategy. We know that GAN training involves alternatively training a discriminator D_{θ_D} and a generator network D_{θ_G} to solve the adversarial min-max problem:

$$\min_{\theta_G} \max_{\theta_D} E_{I^{HR} \sim p_{train}(I^{HR})}\left[\log D_{\theta D}(I^{HR})\right] + E_{I^{LR} \sim p_G(I^{LR})}\left[\log\left(1 - D_{\theta D}\left(G_{\theta_G}(I^{LR})\right)\right)\right] \tag{5}$$

where θ_G and θ_D are the parameters of the generator and discriminator respectively, and $p_{train}(I^{HR})$ is the distribution of target high-resolution images and $p_G(I^{LR})$ is the distribution of the images generated by the

generator. In practice, this is broken down into the loss functions used to first back-propagate through the discriminator network and then the generator.

Loss function of the Discriminator As shown in Equation 5 the Discriminator is trained for the objective

$$\max_{\theta_D} E_{I^{HR}\sim p_{train}(I^{HR})}\left[\log D_{\theta D}(I^{HR})\right] + E_{I^{LR}\sim p_G(I^{LR})}\left[\log\left(1 - D_{\theta D}\left(G_{\theta_G}(I^{LR})\right)\right)\right]$$

or

$$\min_{\theta_D} E_{I^{HR}\sim p_{train}(I^{HR})}\left[\log D_{\theta D}(I^{HR})\right] + E_{I^{LR}\sim p_G(I^{LR})}\left[\log\left(1 - D_{\theta D}\left(G_{\theta_G}(I^{LR})\right)\right)\right]$$

this comes from the formula of binary-cross-entropy (BCE) loss when we label the images I^{HR} as real target value of 1) and label the generated images $G_{\theta_G} I^{LR}$ as fake (target value of 0). We essentially train the Discriminator to identify apart the fake images $I^{SR} = G_{\theta_G} I^{LR}$ from the real images I^{HR}.

Loss fuction of the generator On the other hand, we train the generator to fool the Discriminator such that the Discriminator cannot identify apart the fake images $I^{SR} = G_{\theta_G} I^{LR}$ generated by the generator. This forces the generator to make fake images that look similar to the real ones. In other words, it forces the generator to make the distribution $p_G(I^{LR})$ be similar to the training data distribution $p_{train}(I^{HR})$. Thus, the adversarial loss function l^{SR}_{Gen} (which is the second term in Equation 5) used while training the generator is

$$\begin{aligned} l^{SR}_{Gen} &= \sum_{n=1}^{N} \log\left(1 - D_{\theta_D}\left(G_{\theta_G}(I^{LR})\right)\right) \\ or\ l^{SR}_{Gen} &= \sum_{n=1}^{N} -\log D_{\theta_D}\left(G_{\theta_G}(I^{LR})\right) \end{aligned} \tag{6}$$

This loss function attempts to motivate the generator to create images that the Discriminator would label as real in order to fool the Discriminator. While training the generator though, we add other loss functions, and specifically, the authors of SR-GAN use two additional loss functions, namely: pixel-wise MSE loss l^{SR}_{MSE} and VGG Content loss l^{SR}_{VGG}.

$$l^{SR}_{MSE} = \frac{1}{r^2 WH} \sum_{x=1}^{rW} \sum_{y=1}^{rH} \left(I^{HR}_{x,y} - G_{\theta_G}(I^{LR})_{x,y}\right)^2 \tag{7}$$

$$l^{SR}_{VGG|i.j} = \frac{1}{W_{i,j} H_{i,j}} \sum_{x=1}^{W_{i,j}} \sum_{y=1} \left(\phi_{i,j}(I^{HR})_{x,y} - \phi_{i,j} G_{\theta_G}(I^{LR})_{x,y}\right)^2 \tag{8}$$

Please refer to (Ledig et al., 2017) for details regarding these loss functions. Finally, the loss used to train the generator is l^{SR} named the perceptual loss where $\alpha_1 = 10$, $\alpha_2 = 2\times10^{-6}$, and $\alpha_3 = 10^{-3}$ are scaling factors.

$$l^{SR} = \alpha_1 l^{SR}_{MSE} + \alpha_2 l^{SR}_{VGG} + \alpha_3 l^{SR}_{Gen} \tag{9}$$

These additional loss function terms do not affect the GAN training as similar to l^{SR}_{Gen}, the losses l^{SR}_{MSE} and l^{SR}_{VGG} motivate the generator to make images which are similar to the target distribution $p_{train}(I^{HR})$. In summary,

- l^{SR}_{Gen} motivates the generator to make $p_G(I^{LR})$ similar to $p_{train}(I^{HR})$.
- l^{SR}_{MSE} and l^{SR}_{VGG} motivates the generator to make I^{SR} similar to I^{HR}.

Finally, we can talk about the mass balance loss function $l^{SR}_{MB}\left(I^{LR}, G_{\theta_G}(I^{LR})\right)$. We add this additional term to the perceptual loss

$$l^{SR} = \alpha_1 l^{SR}_{MSE} + \alpha_2 l^{SR}_{VGG} + \alpha_3 l^{SR}_{Gen} + \alpha_4 l^{SR}_{MB}\left(I^{LR}, G_{\theta_G}\left(I^{LR}\right)\right). \quad (10)$$

We argue that $l^{SR}_{MB}\left(I^{LR}, G_{\theta_G}\left(I^{LR}\right)\right)$ too motivates the generator to make $p_G(I^{LR})$ similar to $p_{train}(I^{HR})$ and like the additional terms l^{SR}_{MSE} and l^{SR}_{VGG} does not adversely affect the GAN training. As described above if mass of oil in I^{LR} is equal to that of I^{HR}, then the above argument is true, and the loss function will attempt to make I^{SR} similar to I^{HR}. However, if the masses are not equal then the loss function in combination with l^{SR}_{MSE} and l^{SR}_{VGG} will attempt to make I^{SR} similar to some version $\hat{I}^{HR}$ of I^{HR}, where the mass of oil $\hat{I}^{HR}$ is equal to that of I^{LR}. Although $\hat{I}^{HR} \neq I^{HR}$ but $\hat{I}^{HR}$ will lie in (or very close to) the distribution $p_{train}(I^{HR})$ because any mass corrected version of I^{HR} can be achieved by slightly adjusting the pixel values of the image while still keeping them within [0, 1]. We tune the α_4 to have a very low effect as compared to the other loss components. Also, we initially before even starting the GAN training, we train the generator alone without the mass balance term for a couple of epochs until it performs decent enough for the task of super-resolution reconstruction. When the additional mass balance loss term is added, we do not observe any instability in the min-max GAN training.

Experiments and Results Dataset Generation We want to create a dataset with a wide variety of saturation profiles. Here is a sample data point Figure 4. To that end, we use a very large reservoir model with highly heterogeneous geology and various simulation parameters to generate variety in the saturation profile. For collecting data we use OPM (Open Porous Media). OPM is open-source software, therefore we will be using this in our study. OPM (Rasmussen et al., 2021) flow attempts to reflect reservoir geology, fluid behavior, and well and production facility descriptions in the same way as commercial simulators do, so it includes fully implicit discretization of black-oil style models as well as industry-standard input and output formats. The Fine-scale (FS) model we use is the SPE Model 2. We then crop this model to generate many small fine-scale reservoirs with the following details: Number of Grids: 30 × 110 × 5, Grid Cell Dimension: 20ft × 10ft × 2ft. We then upscale the model (US) with the following details: Number of Grids: 15 × 55 × 5, Grid Cell Dimension: 40ft × 20ft × 2ft. In total (60/30 × 220/110 × 85/5) = 68 reservoir rock configurations are generated from the SPE10 model 2. We also set up one producer well and one injector well with the random location and run the simulation. In total, we change the following parameters: porosity, permeability, producer well location, and injector well location. This results in 6000 models each of FS and US, which were simulated for 20 years.

Generalizability of our Learned Super-Resolution Model We want to emphasize a small detail in the dataset generation process which promotes the generalizability of our model. Recall that our goal is to develop a model which can take a low-resolution saturation profile from the simulation of an up-scaled model and convert it to a high-resolution saturation profile to approximate the results of the corresponding fine-scale simulation. This is done so that a user would not have to run the computationally expensive and time-consuming fine-scale simulation, and yet obtain the approximate fine-scale results from super-resolution of computationally cheaper upscaled simulation. Thus, when we train our model, we want to ensure that the model can generalize to new geology and well conditions, such that anyone can directly use our learned model for their reservoir data without the need to re-train our model for their data.

Because retraining would require them to run training data involving fine-scale simulation results and thus would defeat our purpose. To this end, we investigate three levels:

- First we train the model for fixed geology. This will help us understand the baseline complexity of the problem.
- Next, we change the geology to make the model more generic.
- The saturation profiles however also depend on the operating configuration of the reservoir like well BHP. Thus, finally, we will study how we can make the model generic to these parameters.

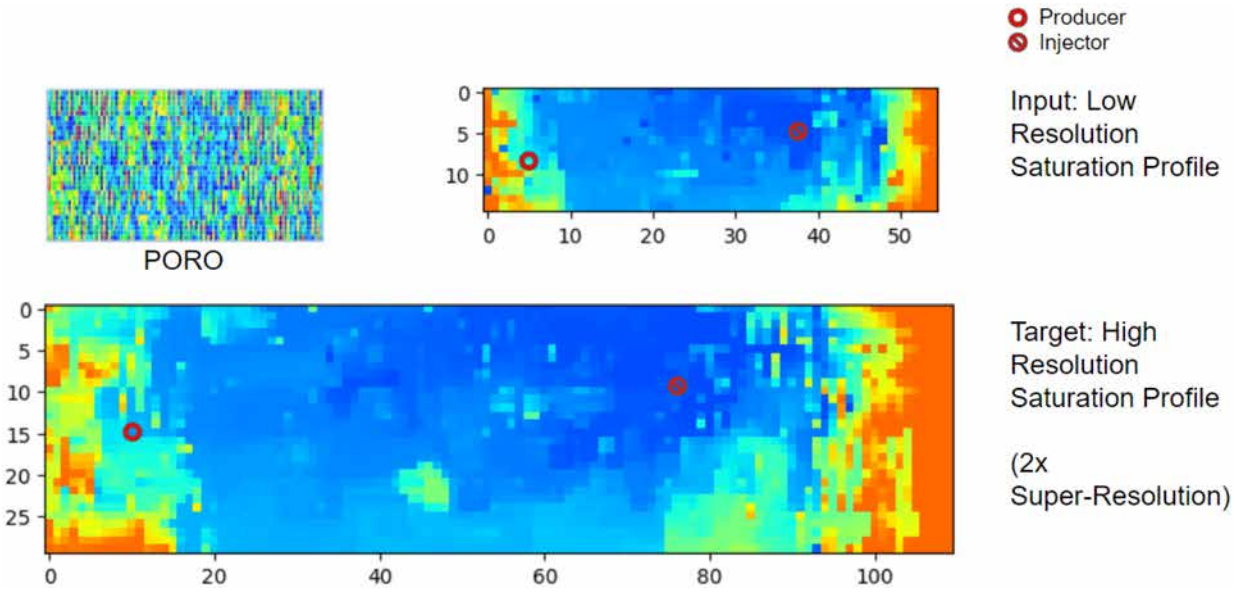

Figure 4—Visualization of a sample Oil Saturation Profile input and the desired high resolution output. We also show the highly non-uniform porosity profile and well locations.

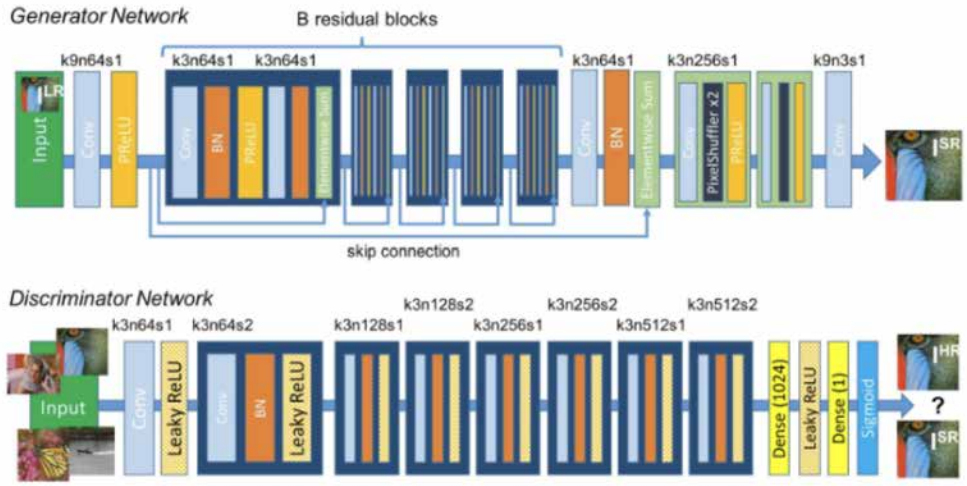

Figure 5—SR-GAN architecture from (Ledig et al., 2017).

The following images Figure 6 show some qualitative examples. The colormap visualization shows the value of saturation at each location of a single reservoir layer. First, we show that the low-resolution profile (LR) lacks a lot of detail as compared to the high-resolution profile (HR). Thus, to reiterate, the goal of my work is to recover the lost details from the low-resolution image. The super-resolution reconstructions (SR-SAN and UNET) are the output of the two models respectively. We can observe that the output of UNet is blurry and lacks details. However, the output of the SR-GAN architecture shows that the model was able to reconstruct the details and generate a reconstruction that is visually very similar to the high-resolution ground truth. This is because Mean based losses used in UNet training trains the network primarily for low-variability features (dominant features which appear across multiple training examples), while the Discriminator based losses used in SR-GAN can make the images also capture high-variability features (features which are more specific to individual training example). From the quantitative analysis Table 1, we observe that the SR-GAN model trained with our dataset works better than a pre-trained SR-GAN model used to reconstruct camera images. This indicates that the super-resolution task involving reservoir data has more domain-specific information which warrants special consideration. The qualitative analysis also

shows that even though the peak signal-to-noise ratio (PSNR) and structural similarity (SSIM) values get reduced upon the introduction of mass balance constraints, the most important value regarding the error in mass balance (M1) reduces significantly.

Table 1—Quantitative results for SR-SAN model.

PSNR: Peak Signal to Noise Ratio (dB)
Higher the better. Camera Image Super-Resolution have ~29
Intuition: How non-blurry and detailed is the output

SSIM: Structural Similarity (%)
Higher the better. Camera Image Super-Resolution have ~90
Intuition: How similar are the super-resolution saturation profile

M1: Percentage error for Mass Balance (Lower the better):
(Mass of SR - Mass of LR)*100 / Mass of LR

M2: (Mass of SR - Mass of HR)*100 / Mass of HR

M3: (Mass of HR - Mass of LR)*100 / Mass of LR

Shaded in Grey are additional information not super important.

Metric	SR-GAN trained on Camera Images	SR-GAN trained on Our Data	SR-GAN trained on Our Data with Mass Balance
PSNR	17.72	24.31	21.51
SSIM	51.79	74.51	66.58
M1 (%)		3.8835	**0.0905**
GMSD	0.1858	0.1110	0.1369
LPIPS	0.3402	0.2696	0.3667
M2 (%)		0.6160	-2.9994
M3 (%)		3.2636	3.2537

Sensitivity of Discriminator to various data-augmentation techniques: As mentioned earlier, we use methods described in (Zhao et al., 2020) to generate augmented datasets with differentiable functions. Here are a list of functions that we attempted and Table 2, summarizes their affect in performance.

Table 2—Performance increase due to various data-augmentation methods.

Data Augmentation Method	Increase in Dataset size	Impact on SSIM
Random Translation	4x	0.91 %
Random Rotation	2x	0.56 %
Random Saturation	5x	26 %
Random global change	2x	17 %

Random Translation: New augmented dataset is created by translating the high-resolution profile by multiple of two, say (2a, 2b) and the corresponding low-resolution profile by (a, b), in both (x, y)-axes respectively. Here a, b are chosen randomly. This translation augmentation helps the network not overfit to spatial patterns specific to the dataset. This augmentation can be used during the discriminator training as it is differentiable.

Random Rotation: Since, the augmented dataset represents underlying physical data that is compartmentalized into three-dimensional grid cells; therefore, rotations that are multiples of 90° degrees are only considered. However, we do not apply this augmentation based on (Zhao et al., 2020) as this augmentation is not differentiable.

Random saturation: We also apply random perturbations in the saturation values as well however, these random perturbations are made such that the total mass of oil is not changed based on Equation 4. In order to do this, we change the porosity of the cell appropriately. We first make the random change in the high-resolution profile and then replicate the same change in porosity and saturation in the low-resolution profile such that the mass of oil is not changed. Again, this transformation is differentiable.

Random global change in oil saturation: We also randomly raise or lower the oil saturation globally in the high-resolution profile and correspondingly adjust the low-resolution profile to ensure mass-balance. Table Table 2 provides the performance difference with each type of data augmentation.

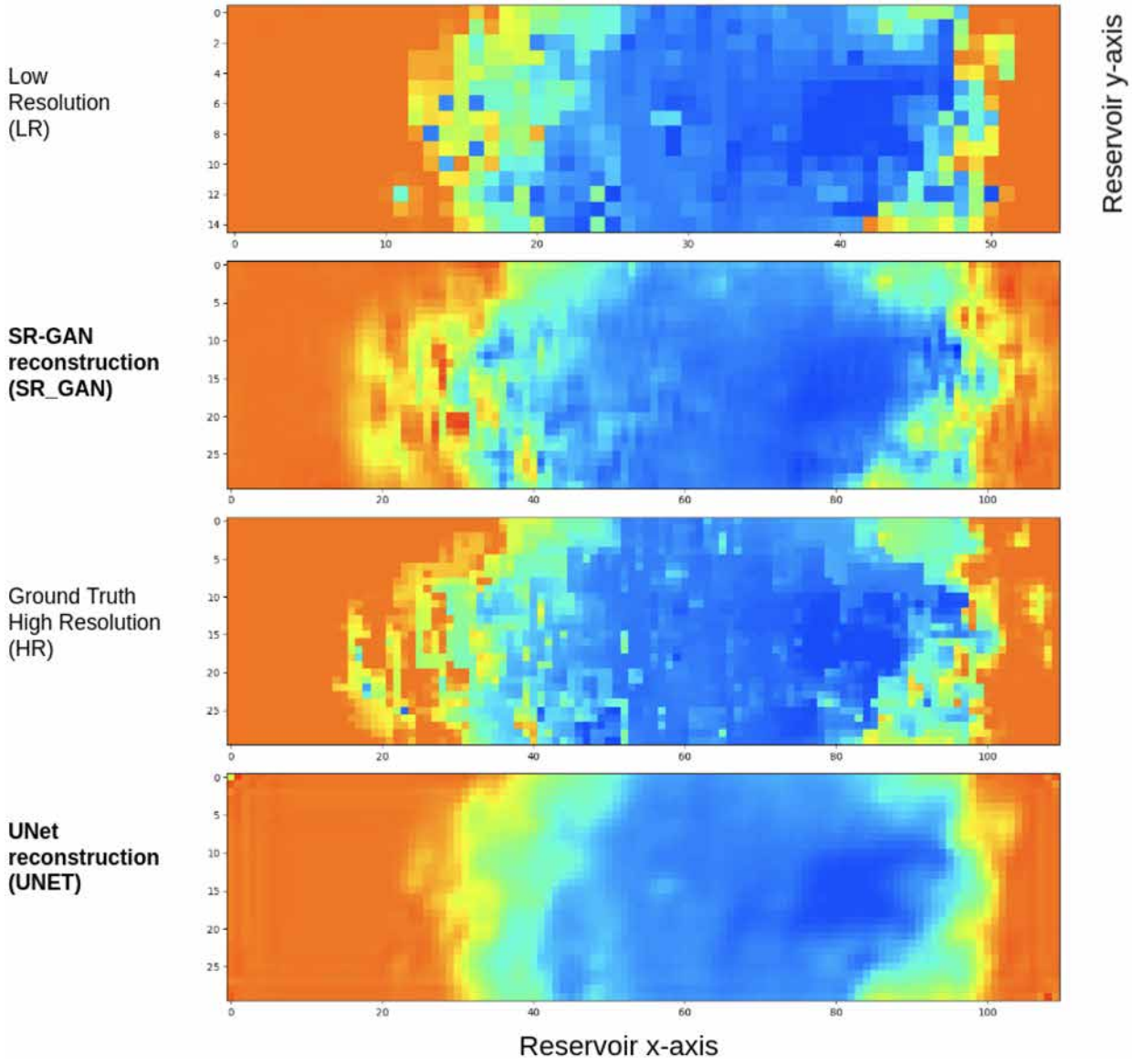

Figure 6—Qualitative result for UNet.

Conclusion

1.The output of the SR-GAN architecture shows that the model was able to reconstruct the details and generate a reconstruction that is visually very similar to the high-resolution ground truth. This is because Mean based losses used in UNet training train the network primarily for low-variability features (dominant features which appear across multiple training examples), while the discriminator based losses used in SR-GAN can make the images also capture high-variability features (features which are more specific to individual training example). 2.From the quantitative analysis, we observe that the SR-GAN model trained with our dataset works better than a pre-trained SR-GAN model used to reconstruct camera images. This indicates that the super-resolution task involving reservoir data has more domain-specific information, which warrants special consideration. 3.The qualitative analysis also shows that even though the peak signal-to-noise ratio (PSNR) and structural similarity (SSIM) values get reduced upon the introduction of mass

balance constraints, the most important value regarding the error in mass balance (M1) reduces significantly. In this work we only upscaled saturation but another key dynamic property is pressure. So in future work we will explore how we can perform super resolution for both pressure and saturation together, while making sure that physical constraint are met.

Acknowledgement

I appreciate the thoughtful criticism provided by the Carnegie Mellon University anonymous peer reviewers. The kindness and knowledge of everyone have helped this study in countless ways and prevented me from making many mistakes; those that unavoidably remain are solely my responsibility.

References

Ahmadi, M. A., Ebadi, M., Shokrollahi, A., and Majidi, S. M. J. (2013). Evolving artificial neural network and imperialist competitive algorithm for prediction oil flow rate of the reservoir. *Applied Soft Computing*, **13**(2):1085–1098.

Bode, M., Gauding, M., Kleinheinz, K., and Pitsch, H. (2019). Deep learning at scale for subgrid modeling in turbulent flows: regression and reconstruction. *In International Conference on High Performance Computing*, pages 541–560. Springer.

Britto, A., Vivas, C., Almeida, M., da Cunha Lima, I., and da Cunha Lima, A. (2020). Multiphase flow mobility impact on oil reservoir recovery: An open-source simulation. *AIP Advances*, **10**(3):035032.

Brouwer, G. and Fokker, P. (2013). Upscaling and downscaling with an effective medium theory, applied to heterogeneous reservoir. In EAGE Annual Conference & Exhibition incorporating SPE Europec. OnePetro.

Cai, S., Mao, Z., Wang, Z., Yin, M., and Karniadakis, G. E. (2022). Physics-informed neural networks (pinns) for fluid mechanics: A review. *Acta Mechanica Sinica*, pages 1–12.

Cao, Q., Banerjee, R., Gupta, S., Li, J., Zhou, W., and Jeyachandra, B. (2016). Data driven production forecasting using machine learning. *Society of Petroleum Engineers - SPE Argentina Exploration and Production of Unconventional Resources Symposium*.

Castelletti, A., Galelli, S., Restelli, M., and Soncini-Sessa, R. (2010). Tree-based reinforcement learning for optimal water reservoir operation. *Water Resources Research*, **46**(9).

Chaudhuri, S. (2001). Super-resolution imaging, volume **632**. Springer Science & Business Media.

Da Wang, Y., Blunt, M. J., Armstrong, R. T., and Mostaghimi, P. (2021). Deep learning in pore scale imaging and modeling. *Earth-Science Reviews*, page 103555.

Das, M. P., Conover, D. M., Eum, S., Kwon, H., and Likhachev, M. (2022). Ma3: Model-accuracy aware anytime planning with simulation verification for navigating complex terrains. *In Proceedings of the International Symposium on Combinatorial Search*, volume **15**, pages 65–73.

Das, M. P., Matthies, L., and Daftry, S. (2021). Online photometric calibration of automatic gain thermal infrared cameras. *IEEE Robotics and Automation Letters*, **6**(2):2453–2460.

Demiryurek, U., Banaei-Kashani, F., Shahabi, C., and Wilkinson, F. G. (2008). Neural-network based sensitivity analysis for injector-producer relationship identification. In Intelligent Energy Conference and Exhibition. OnePetro.

Dong, C., Loy, C. C., He, K., and Tang, X. (2015). Image super-resolution using deep convolutional networks. *IEEE transactions on pattern analysis and machine intelligence*, **38**(2):295–307.

Fukami, K., Fukagata, K., and Taira, K. (2019). Super-resolution reconstruction of turbulent flows with machine learning. *Journal of Fluid Mechanics*, **870**:106–120.

Holdaway, K. R. (2014). Harness oil and gas big data with analytics: Optimize exploration and production with data-driven models. John Wiley & Sons.

Janssens, N., Huysmans, M., and Swennen, R. (2020). Computed tomography 3d super-resolution with generative adversarial neural networks: implications on unsaturated and two-phase fluid flow. *Materials*, **13**(6):1397.

Jia, P., Zhang, M., Yu, W., Shen, F., and Shen, Y. (2016). Convolutional neural network based classification for hyperspectral data. In 2016 IEEE International Geoscience and Remote Sensing Symposium (IGARSS), pages 5075–5078. IEEE.

Karpatne, A., Watkins, W., Read, J., and Kumar, V. (2017). How can physics inform deep learning methods in scientific problems?: Recent progress and future prospects. In 31st Conference on Neural Information Processing Systems (NeurIPS), pages 1–5.

Lantz, B. (2019). Machine learning with R: expert techniques for predictive modeling. Packt Publishing Ltd.

Ledig, C., Theis, L., Husz´ar, F., Caballero, J., Cunningham, A., Acosta, A., Aitken, A., Tejani, A., Totz, J., Wang, Z., et al (2017). Photo-realistic single image super-resolution using a generative adversarial network. *In Proceedings of the IEEE conference on computer vision and pattern recognition*, pages 4681–4690.

Liu, C. and McVay, D. A. (2010). Continuous reservoir-simulation-model updating and forecasting improves uncertainty quantification. *SPE Reservoir Evaluation and Engineering*, **13**(4):626–637.

Maula, A., Rofieq, S., Sabila, T., Lestariono, Y., et al (2020). Artificial neural network surrogate reservoir proxy modeling for generating pressure and gas saturation at the grid–block level in shale gas reservoirs. In Offshore Technology Conference Asia. Offshore Technology Conference.

Panda, M., Chopra, A., et al (1998). An integrated approach to estimate well interactions. In SPE India Oil and Gas Conference and Exhibition. Society of Petroleum Engineers.

Pant, P. and Farimani, A. B. (2020). Deep learning for efficient reconstruction of high-resolution turbulent dns data. arXiv preprint arXiv:2010.11348.

Rahm, E. and Do, H. H. (2000). Data cleaning: Problems and current approaches. *IEEE Data Eng. Bull.*, **23**(4):3–13.

Rasmussen, A. F., Sandve, T. H., Bao, K., Lauser, A., Hove, J., Skaflestad, B., Kl¨ofkorn, R., Blatt, M., Rustad, A. B., Sævareid, O., Lie, K. A., and Thune, A. (2021). The Open Porous Media Flow reservoir simulator. *Computers and Mathematics with Applications*, **81**:159–185.

Ronneberger, O., Fischer, P., and Brox, T. (2015). U-net: Convolutional networks for biomedical image segmentation. *In International Conference on Medical image computing and computer-assisted intervention*, pages 234–241. Springer.

Torrealba, V. A., Hoteit, H., Chawathe, A., et al (2019). Improving chemical-enhanced-oil-recovery simulations and reducing subsurface uncertainty using downscaling conditioned to tracer data. *SPE Reservoir Evaluation & Engineering*, **22**(04):1–426.

Wang, X., Yu, K., Wu, S., Gu, J., Liu, Y., Dong, C., Qiao, Y., and Change Loy, C. (2018a). Esrgan: Enhanced super-resolution generative adversarial networks. In Proceedings of the European Conference on Computer Vision (ECCV) Workshops, pages 0–0.

Wang, Y., Rahman, S. S., and Arns, C. H. (2018b). Super resolution reconstruction of µ-ct image of rock sample using neighbour embedding algorithm. *Physica A: Statistical Mechanics and its Applications*, **493**:177–188.

Wang, Y., Teng, Q., He, X., Feng, J., and Zhang, T. (2019). Ct-image of rock samples super resolution using 3d convolutional neural network. *Computers & Geosciences*, **133**:104314.

Wuest, T., Weimer, D., Irgens, C., and Thoben, K.-D. (2016). Machine learning in manufacturing: advantages, challenges, and applications. *Production & Manufacturing Research*, **4**(1):23–45.

Xie, Y., Franz, E., Chu, M., and Thuerey, N. (2018). tempogan: A temporally coherent, volumetric gan for super-resolution fluid flow. *ACM Transactions on Graphics (TOG)*, **37**(4):1–15.

Yu, S., Zhu, K., and Diao, F. (2008). A dynamic all parameters adaptive bp neural networks model and its application on oil reservoir prediction. *Applied mathematics and computation*, **195**(1):66–75.

Zhao, S., Liu, Z., Lin, J., Zhu, J.-Y., and Han, S. (2020). Differentiable augmentation for data-efficient gan training. *Advances in Neural Information Processing Systems*, **33**:7559–7570.